Single-crystal vs polycrystalline boron-doped diamond anodes

Comparing degradation efficiencies of carbamazepine in electrochemical water treatment

Feijoo, Sara; Baluchová, Simona; Kamali, Mohammadreza; Buijnsters, Josephus G.; Dewil, Raf

DOI
10.1016/j.envpol.2024.123705

Publication date
2024

Document Version
Final published version

Published in
Environmental Pollution

Environmental Pollution 347 (2024) 123705

Contents lists available at ScienceDirect

Environmental Pollution

journal homepage: www.elsevier.com/locate/envpol

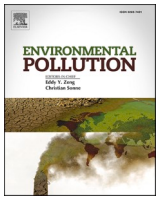

Single-crystal vs polycrystalline boron-doped diamond anodes: Comparing degradation efficiencies of carbamazepine in electrochemical water treatment☆

Sara Feijoo [a], Simona Baluchová [b,c], Mohammadreza Kamali [a], Josephus G. Buijnsters [b,*], Raf Dewil [a,d]

[a] KU Leuven, Department of Chemical Engineering, Process and Environmental Technology Lab, Jan Pieter de Nayerlaan 5, 2860, Sint-Katelijne-Waver, Belgium
[b] Delft University of Technology, Department of Precision and Microsystems Engineering, Mekelweg 2, 2628 CD, Delft, the Netherlands
[c] Charles University, Faculty of Science, Department of Analytical Chemistry, Albertov 6, 128 00, Prague, Czech Republic
[d] University of Oxford, Department of Engineering Science, Parks Road, Oxford, OX1 3PJ, United Kingdom

ARTICLE INFO

Handling editor: Amit Bhatnagar

Keywords:
Electrochemical advanced oxidation processes (eAOPs)
boron-doped diamond (BDD)
single-crystal
polycrystalline
wastewater treatment

ABSTRACT

The ongoing challenge of water pollution by contaminants of emerging concern calls for more effective wastewater treatment to prevent harmful side effects to the environment and human health. To this end, this study explored for the first time the implementation of single-crystal boron-doped diamond (BDD) anodes in electrochemical wastewater treatment, which stand out from the conventional polycrystalline BDD morphologies widely reported in the literature. The single-crystal BDD presented a pure diamond (sp^3) content, whereas the three other investigated polycrystalline BDD electrodes displayed various properties in terms of boron doping, sp^3/sp^2 content, microstructure, and roughness. The effects of other process conditions, such as applied current density and anolyte concentration, were simultaneously investigated using carbamazepine (CBZ) as a representative target pollutant. The Taguchi method was applied to elucidate the optimal operating conditions that maximised either (i) the CBZ degradation rate constant (enhanced through hydroxyl radicals ($^{\bullet}OH$)) or (ii) the proportion of sulfate radicals ($SO_4^{\bullet-}$) with respect to $^{\bullet}OH$. The results showed that the single-crystal BDD significantly promoted $^{\bullet}OH$ formation but also that the interactions between boron doping, current density and anolyte concentration determined the underlying degradation mechanisms. Therefore, this study demonstrated that characterising the BDD material and understanding its interactions with other process operating conditions prior to degradation experiments is a crucial step to attain the optimisation of any wastewater treatment application.

1. Introduction

To remediate the pollution associated with the presence of recalcitrant micropollutants in natural water bodies (Rizzo et al., 2019), electrochemical advanced oxidation processes (eAOPs) have been widely investigated as a promising wastewater treatment method (Ganiyu et al., 2021). The effectiveness of electrochemical wastewater treatment is related to the generation of highly reactive species, such as hydroxyl ($^{\bullet}OH$) and sulfate radicals ($SO_4^{\bullet-}$), to degrade micropollutants (Scaria and Nidheesh, 2022). In recent years, $SO_4^{\bullet-}$ have gained scientific interest because of their longer half-life in wastewater and their high redox potential in a wider pH range (Scaria and Nidheesh, 2022; Duan et al., 2022), especially because of the possibility of being generated from sulfate ions (SO_4^{2-}), an ionic species ubiquitously found in wastewater effluents (Radjenovic and Petrovic, 2017). As such, the formation of $SO_4^{\bullet-}$ can be attained via non-active electrode materials such as boron-doped diamond (BDD) (Eqs. (1) and (2)), in combination with the generation of $^{\bullet}OH$ from water molecules (Eq. (3)) (Li et al., 2022a; Divyapriya and Nidheesh, 2021; Araújo et al., 2022). These radical formation mechanisms are commonly referred to as "in situ" and present the added value that no additional chemical precursors are necessary to carry out pollutant degradation (Araújo et al., 2022). In addition, BDD anodes bring other advantageous characteristics to the table, such as

☆ This paper has been recommended for acceptance by Amit Bhatnagar.

* Corresponding author.
E-mail address: j.g.buijnsters@tudelft.nl (J.G. Buijnsters).

https://doi.org/10.1016/j.envpol.2024.123705
Received 16 November 2023; Received in revised form 21 February 2024; Accepted 2 March 2024
Available online 3 March 2024

Abbreviations

AFM	Atomic force microscopy
ANOVA	Analysis of variance
AOP(s)	Advanced oxidation process(es)
BDD	Boron-doped diamond
CBZ	Carbamazepine
CV	Cyclic voltammetry
DoF	Degrees of freedom
eAOP(s)	Electrochemical advanced oxidation process(es)
Mean Sq	Mean of squares
MeOH	Methanol
OER	Oxygen evolution reaction
SEM	Scanning electron microscopy
S/N	Signal-to-noise ratio
Sum Sq	Sum of squares
tBuOH	Tert-butanol
UHPLC	Ultra-high performance liquid chromatography

their high stability, wide potential window, and a "non-active" nature that favours oxidation reactions over adsorption and desorption mechanisms (Divyapriya and Nidheesh, 2021; Garcia-Segura et al., 2015; Suresh et al., 2022; Preethi et al., 2023).

$$BDD + SO_4^{2-} \rightarrow BDD\left(SO_4^{\bullet-}\right) + e^- \quad (1)$$

$$BDD(^{\bullet}OH) + SO_4^{2-} \rightarrow BDD\left(SO_4^{\bullet-}\right) + OH^- \quad (2)$$

$$BDD + H_2O \rightarrow BDD(^{\bullet}OH) + H^+ + e^- \quad (3)$$

The formation of oxidative radicals is, however, not tied to a specific set of operating conditions, as the selected electrolyte, wastewater composition, electrode material and applied current density are known factors affecting the overall treatment performance (Ganiyu et al., 2021; Yakamercan et al., 2023). Out of these design considerations, the BDD material properties are often overlooked by researchers when optimising wastewater treatment applications, yet recent studies have confirmed that features such as the sp^3 (i.e., diamond) and sp^2 (i.e., graphitic carbon) content ratio, substrate material and boron doping can strongly influence the underlying electron transfer kinetics (Garcia-Segura et al., 2015; de Paiva et al., 2015; Brito et al., 2018). For instance, both a higher sp^3 content and utilising niobium as a substrate material were reported to favour the generation of $^{\bullet}OH$ (Garcia-Segura et al., 2015; Brito et al., 2018), whereas a higher sp^2 content enhanced adsorption sites for SO_4^{2-} and thus $SO_4^{\bullet-}$ formation (de Paiva et al., 2015). During the degradation of enrofloxacin and rhodamine B, a higher sp^2 content was observed to favour direct oxidation mechanisms at the anode surface and the formation of more reaction intermediates, in contrast to the complete pollutant mineralisation attained with higher sp^3 contents (Guinea et al., 2009; Medeiros de Araújo et al., 2014). When further evaluating these findings in wastewater pollution remediation studies, the available body of literature is nonetheless rather limited (Guinea et al., 2009; Medeiros de Araújo et al., 2014; Cañizares et al., 2008; da Silva et al., 2018), mostly due to the complexity that in-house BDD electrode fabrication, characterisation and modification entail.

As a result, acquiring a commercially available BDD electrode is common practice among researchers. The majority of these BDD anodes present a polycrystalline character with diverse crystal facets that expose the diamond grains, leading to a heterogeneous distribution of surface properties, such as boron doping, polarity and sp^2 carbon impurities (Liu et al., 2023). This heterogeneity can significantly affect the BDD electrochemical properties, which also determine the interactions with pollutants and electrolytes during degradation experiments (Liu et al., 2023). To this end, single-crystal BDDs have been recently explored as an alternative electrode material consisting of a conductive diamond layer with a specific composition and orientation (Liu et al., 2023; Ivandini et al., 2019; Čambal et al., 2023). In a previous study, Liu et al. (2023) investigated the differences in electrochemical properties that arise when comparing BDD layers grown on heteroepitaxial diamond quasi-substrates (i.e., single-crystal BDD) and conventional polycrystalline BDD. Their work revealed that heteroepitaxial single-crystal BDDs exhibited faster electron transfer kinetics, wide potential windows and low double-layer capacitance values, as well as circumvented the presence of sp^2 impurities, and thus showed improved electrochemical performance.

In this research, the previously observed differences between polycrystalline and single-crystal BDD electrodes were further evaluated for the degradation of a common micropollutant in wastewater: carbamazepine (CBZ), an anticonvulsant frequently used to treat epilepsy (Beydoun et al., 2020; Wilkinson et al., 2022). In addition, the influence of the initial concentration of SO_4^{2-} in the wastewater and the current density applied were taken into consideration. For each CBZ degradation scenario, the contributions of $^{\bullet}OH$ and $SO_4^{\bullet-}$ were estimated by scavenging tests, and two optimisation analyses were conducted, aiming to maximise (i) the CBZ degradation rate constant and (ii) the proportion of $SO_4^{\bullet-}$ in relation to $^{\bullet}OH$. As a result, this work sheds light on the optimal operating conditions (i.e., initial SO_4^{2-} concentration, current density, and electrode properties) that may favour sulfate radical-based eAOP treatments.

2. Materials & methods

2.1. Chemicals

Carbamazepine ($C_{15}H_{12}N_2O$, CBZ, ≥98%) was purchased from Sigma–Aldrich (Germany). Sodium sulfate (Na_2SO_4, 99%), tert-butanol ($(CH_3)_3COH$, 99.5%) and methanol (CH_3OH, 99.8% for HPLC) were acquired from Acros Organics (Belgium) as well as acetonitrile (CH_3CN, ≥99.9%) and formic acid (CH_2O_2, ≥98% for analysis) for UHPLC analysis. Working solutions were prepared with Milli-Q water purified using a Milli-Q®-Reference system (18 MΩ cm) from Merck (Germany).

2.2. Experimental setup

Degradation experiments were performed in a 200 mL undivided laboratory-scale electrochemical cell containing two electrode holders made of PEEK material. For the working electrode or anode, a flat specimen holder was used, presenting a circular aperture of 8 mm in diameter on the front side (Redox.me, Sweden), which defined the geometrical electrode area of 0.50 cm^2. The back of the anode was in contact with a copper foil (not exposed to the electrolyte), which ensured optimal current collection and distribution. In this holder, 4 different types of BDD electrodes were investigated: (i) a 10 × 10 mm^2 free-standing heteroepitaxial single-crystal BDD with a polished top growth side (SC-BDD), (ii) a 15 × 15 mm^2 free-standing polycrystalline BDD with distinctive nucleation (Poly-BDD-N) and (iii) polished growth (Poly-BDD-G) sides supplied by Mintres B.V. (The Netherlands), and (iv) a commercial polycrystalline BDD film (Poly-BDD-C) from Metrohm (Belgium). The counter electrode or cathode was a stainless steel electrode with dimensions of 72 × 20 × 1 mm^3, of which a surface of 53 × 20 × 1 mm^3 was immersed in the water solution and exposed on both sides. Its holder was made of a tantalum contact and a PEEK screw to fix the electrode to the wire contact (Redox.me, Sweden). The reference electrode was Ag/AgCl (+0.210 V vs SHE), placed in the vicinity of the working electrode. The interelectrode distance was fixed at 40 mm. Chronopotentiometry experiments were conducted with a potentiostat/galvanostat AUT302N.S PGSTAT302N acquired from Metrohm (Belgium). At given time intervals, 1 mL samples were collected, filtered with a high-grade syringe filter (CHROMAFIL® Xtra PET, 25 mm diameter, 0.2 μm pore size, Macherey-Nagel, Germany) and

subsequently quenched with 500 μL UHPLC-grade methanol to prevent further degradation reactions. Experiments were performed at least in duplicate and conducted in batch mode at room temperature with constant magnetic stirring at 400 rpm.

2.3. Electrode characterisation techniques

The surface morphology of all employed BDD electrodes was visualised by a scanning electron microscope (JSM6500F, JEOL, USA) in secondary electron imaging mode operated at 15 keV. Raman spectroscopy was performed at room temperature using a Horiba LabRAM HR device equipped with a solid state Cobolt Fandango™ laser operating at a 515 nm wavelength (Hübner Photonics, Germany) to assess the BDD layer composition. The fitting tool described by Mortet et al. (2020) and available at https://ramantool.pythonanywhere.com/ was used over the range of 1100–1500 cm^{-1} to estimate the boron concentration ([B], cm^{-3}) from Raman spectra. Mean surface roughness (S_a, nm) was assessed from atomic force microscopy (AFM) measurements conducted with a JPK Nanowizard 4 (Bruker, USA) in tapping mode with silicon tips over a scanned area of 60 μm × 60 μm.

2.4. Chemical analysis

The concentration of CBZ was monitored over time with an ultra-high performance liquid chromatography (UHPLC) instrument (1260 Infinity II, Agilent Technologies, Germany) according to the chromatographic method developed by Jiang et al. (2019).

2.5. Design of experiments & data analysis

Degradation curves were modelled under pseudo-first order kinetics and fitted by non-linear regressions, while the elucidation of the optimal conditions was carried out through the Taguchi method in combination with analysis of variance (ANOVA) (Feijoo et al., 2022a). The Taguchi method is based on standard orthogonal arrays to identify the optimal combinations of process factors (i.e., parameters) at distinct values (i.e., levels) to reach an optimisation target (Mandal et al., 2011). In this study, 3 parameters (i.e., electrode material, initial SO_4^{2-} concentration, and current density) were investigated for the degradation of 100 μg L^{-1} CBZ, which is a plausible concentration in municipal wastewater effluents (i.e., maximum concentration reported to be 259 μg L^{-1} (NORMAN-Network, 2021)). The electrode material was evaluated for 4 levels (i.e., SC-BDD, Poly-BDD-N, Poly-BDD-G, and Poly-BDD-C), while the initial SO_4^{2-} concentration and current density were set at 2 levels. The selected SO_4^{2-} concentrations were 250 and 500 mg L^{-1}, as the former corresponds to the EU concentration limit in drinking water (European Commission, 2022), and the latter can be found in wastewater effluents (Feijoo et al., 2022b; Li et al., 2022b). The current density was evaluated at 5 and 50 mA cm^{-2}, given that the former has already been proven to degrade CBZ (Feijoo et al., 2022a) and the latter is of interest due to the possibly higher degradation efficiencies attained. Consequently, the Taguchi L8b design was implemented in this work (Table 1).

To quantify the contribution of $SO_4^{\bullet-}$ or $^{\bullet}OH$ in each Taguchi experiment, separate scavenging tests were performed. In these tests, either tert-butanol or methanol was added to the reaction mixture, as the former inhibits only $^{\bullet}OH$ and the latter scavenges both $^{\bullet}OH$ and $SO_4^{\bullet-}$ (Wang and Wang, 2020). These scavenging tests were performed likewise to those in Table 1, with the addition of tert-butanol and methanol in a molar ratio of 1000:1 with respect to CBZ (Feijoo et al., 2022a). Based on the degradation kinetics retrieved in the Taguchi experiments (denoted as k) and in the scavenging tests with tert-butanol (denoted as k_t) and methanol (denoted as k_m), the contributions of $^{\bullet}OH$ and $SO_4^{\bullet-}$ were estimated through Eqs. (4) and (5), respectively.

$$\%^{\bullet}OH = (k\text{-}k_t)/(k\text{-}k_m) \quad (4)$$

Table 1
Experimental scenarios according to the Taguchi L8b design.

Experiment	Electrode	CBZ (μg L^{-1})	SO_4^{2-} (mg L^{-1})	Current density (mA cm^{-2})
T1	SC-BDD	100	250	5
T2	SC-BDD	100	500	50
T3	Poly-BDD-N	100	250	5
T4	Poly-BDD-N	100	500	50
T5	Poly-BDD-G	100	500	5
T6	Poly-BDD-G	100	250	50
T7	Poly-BDD-C	100	500	5
T8	Poly-BDD-C	100	250	50

$$\%SO_4^{\bullet-} = 1\text{-}\%^{\bullet}OH \quad (5)$$

As a result, two Taguchi optimisation scenarios were conducted to maximise (i) the overall CBZ degradation rate constant and (ii) the proportion of $SO_4^{\bullet-}$ with respect to $^{\bullet}OH$ (Eq. (6)). In each scenario, the Taguchi signal-to-noise ratio (S/N) was calculated under the "higher-the-better" definition (Eq. (7)), where y and n are the experimental observations and their number, respectively (Ogulata and Mezarcioz, 2011). Calculations were performed with RStudio® software version April 1, 1103 (R Core Team, 2023).

$$P_{SO4\bullet-} = \left(\%SO_4^{\bullet-}\text{-}\%^{\bullet}OH\right) / |\,\%^{\bullet}OH\,| \quad (6)$$

$$S/N = -10\log\left(\frac{1}{n}\sum_{i=1}^{n}\frac{1}{y_i^2}\right) \quad (7)$$

3. Results

3.1. Morphological and structural characterisation

3.1.1. Scanning electron microscopy (SEM)

The morphological characteristics of the BDD electrodes were observed via SEM. The acquired micrographs are depicted in Fig. 1 together with schematic representations of the BDD surface compositions. As observed in the micrographs, significant differences in the domain (grain) size, mean surface roughness (S_a) and grain boundaries density can be recognised among the BDD samples, which are also quantified and summarised in Table 2. Besides, the SEM images were subjected to a surface fractal analysis (using Fractal Dimension Estimator software employing the box count method) and the fractal dimension values in a range of 2.03–2.07 were obtained for the investigated BDD electrodes.

As shown in Fig. 1a, the characteristics of the SC-BDD surface, consisting of only one grain domain, are dominated by polishing lines. Their presence is the consequence of rough mechanical polishing; however, the surface remained very flat (~4 nm). The other three studied BDD electrodes are polycrystalline in nature, and their heterogeneous surfaces are composed of diamond grains differing in size and crystal orientation and related boundary regions. The recorded SEM images, displayed in Fig. 1b–d, show significant variations in the morphological features of the polycrystalline BDD electrodes. In particular, concerning the free-standing BDD electrode, the Poly-BDD-G surface (Fig. 1b) is composed of large crystals with diameters reaching tens of μm, while the smallest average grain size (~1 μm) is recognised for the Poly-BDD-N sample (Fig. 1c). Such differences in grain size translate naturally into the number of grain boundaries, which is significantly higher on the Poly-BDD-N surface. A common feature of both Poly-BDD-G and Poly-BDD-N is the very high smoothness (~5 nm) of their surfaces, even

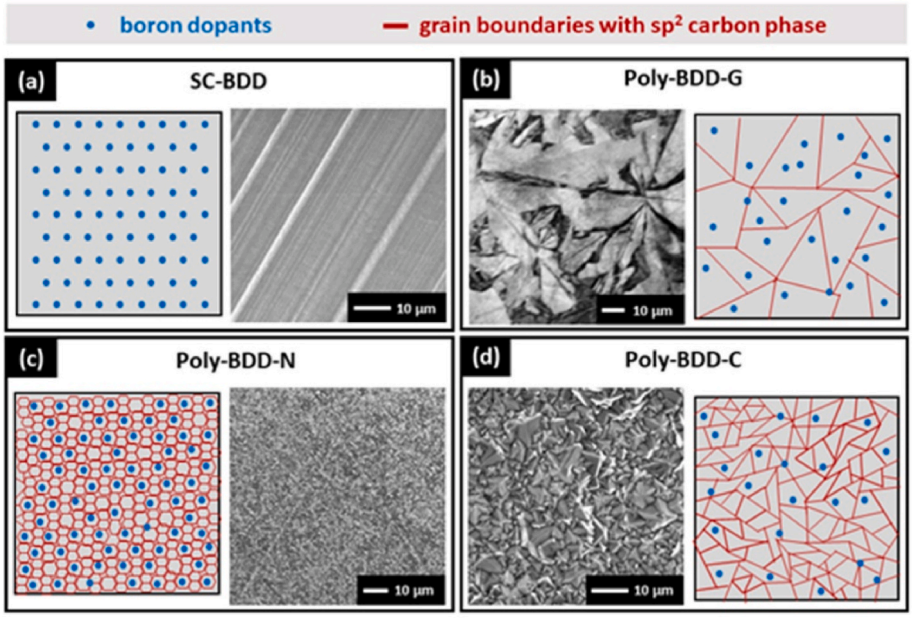

Fig. 1. SEM images and schematic representations of the surface textures and compositions of the (a) SC-BDD, (b) Poly-BDD-G, (c) Poly-BDD-N and (d) Poly-BDD-C electrodes.

Table 2
Morphological, structural and electrochemical characteristics of the BDD electrodes.

BDD electrode	Domain size (µm)	S_a (nm)	[B] (cm^{-3})	sp^2 content
SC-BDD	10,000	3.9	$2.7 \cdot 10^{21}$	negligible
Poly-BDD-G	4–55	5.2	$7.7 \cdot 10^{19}$	negligible
Poly-BDD-N	0.5–2	5.1	$5.6 \cdot 10^{20}$	significant
Poly-BDD-C	1.5–8	>100	$8.4 \cdot 10^{19}$	significant

comparable with SC-BDD, as a result of mechanical polishing. In contrast, the highest surface roughness (>100 nm) is recognised for the Poly-BDD-C layer (Fig. 1d), which is available in its "as-grown" state, as it was not subjected to any polishing treatment. In addition, the thin-film BDD of Poly-BDD-C, deposited on a silicon substrate, is characterised by a grain size ranging from 1 to 10 µm with related and quite dense intergrain regions.

3.1.2. Raman spectroscopy

Non-destructive Raman spectroscopy was employed to assess the quality and composition of the various BDD electrodes. Representative Raman spectra recorded for each electrode are depicted in Fig. 2, and as expected, they considerably differ depending on the amount of incorporated boron atoms and sp^2 carbon (Table 2).

The common, and simultaneously the most prominent, feature of all four spectra is the sharp diamond's zone centre phonon line located in the range of 1329–1332 cm^{-1}. In addition, SC-BDD and Poly-BDD-N manifest typical features of heavily B-doped diamond (with B concentrations above 10^{20} cm^{-3}), as evident in Fig. 2a and c: (i) the intense broad band centred at 490 cm^{-1} originating from the combination of electronic Raman scattering and a Fano-shaped band (Mortet et al., 2020), and (ii) the asymmetric band developed at ~1220 cm^{-1} due to the phonon density of states (Sidorov and Ekimov, 2010). Both characteristic bands are much less pronounced in the spectra of Poly-BDD-G and Poly-BDD-C, which signal a lower degree of boron incorporation in these diamond materials. This was further confirmed by the fitting tool described in section 2.3, which evaluated [B] for the Poly-BDD-G and Poly-BDD-C electrodes at the level of ~$8 \cdot 10^{19}$ cm^{-3}, while much higher boron doping was assessed for the Poly-BDD-N and SC-BDD samples (Table 2).

Moreover, the pronounced G-band arising at ~1550 cm^{-1} in the Raman spectra of Poly-BDD-N and Poly-BDD-C (Fig. 2c and d) suggests the presence of a graphitic phase (sp^2-hybridised carbon), residing predominantly in the boundary areas. These results correlate well with the previous observations made by SEM, discussed in section 3.1.1, where the smallest diamond grains, and thus the highest density of boundaries, were identified for the Poly-BDD-N and Poly-BDD-C electrodes (Fig. 1c–d). In contrast, the barely developed G-band in the spectra of SC-BDD and Poly-BDD-G indicates that these electrodes are largely free of sp^2 carbon impurities (only negligible to very low amounts are present) and hence possess a very high phase purity.

Notably, the parameters such as boron dopant concentration and presence of sp^2 carbon phase largely affect the electrochemical behaviour of the BDD electrodes and their performance in the degradation experiments, as discussed in detail in Section 3.2. Besides, these parameters determine the electroactive area of the BDD electrodes, which is expected to be smaller (averagely by 10–15%) than their geometrical area. This is attributed to the fact that not the whole BDD surface is electroactive but both inactive and highly electrochemically active regions coexist together, as recently demonstrated for the Poly-BDD-G electrode in (Liu et al., 2024). However, for comparison purposes, a well-defined geometrical area, same for all BDD electrodes, was considered in the current density parameter in this work.

3.2. Experimental results: radical contributions during CBZ degradation

After conducting the eight degradation experiments described in Table 1 together with the corresponding scavenging tests with tert-butanol and methanol, their pseudo-first order kinetic constants were retrieved through non-linear modelling (Fig. A1) and used to estimate radical contributions. An overview of these estimations is provided in Fig. 3, where specific comparisons between electrode types can be drawn for experiments with common values for current density and SO_4^{2-} concentration. In addition, the UHPLC chromatograms of each experiment (Fig. A2) were evaluated in terms of the detected CBZ degradation products (Fig. 4).

From a radical contributions point of view, the single-crystal BDD (i.e., SC-BDD) used in experiments Taguchi 1 and Taguchi 2 exhibited

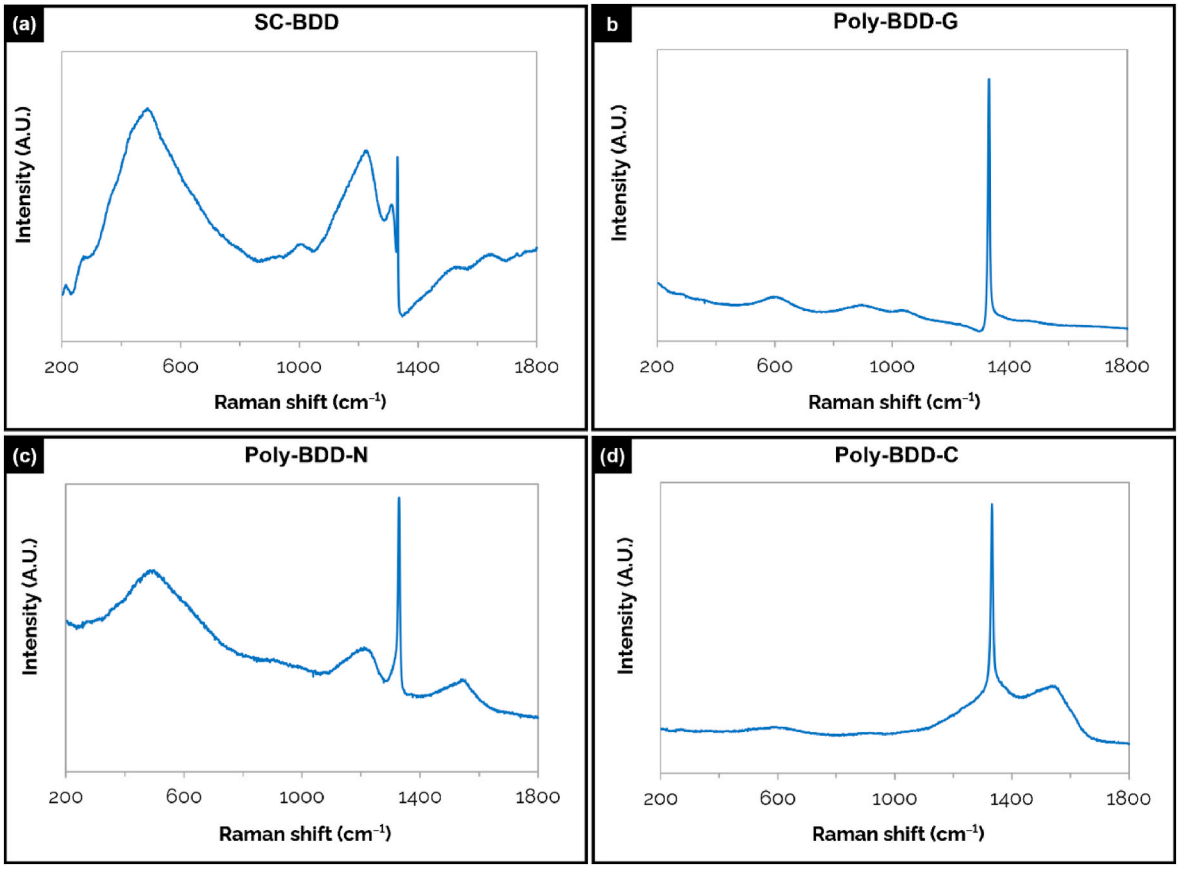

Fig. 2. Raman spectra recorded for the (a) SC-BDD, (b) Poly-BDD-G, (c) Poly-BDD-N and (d) Poly-BDD-C electrodes.

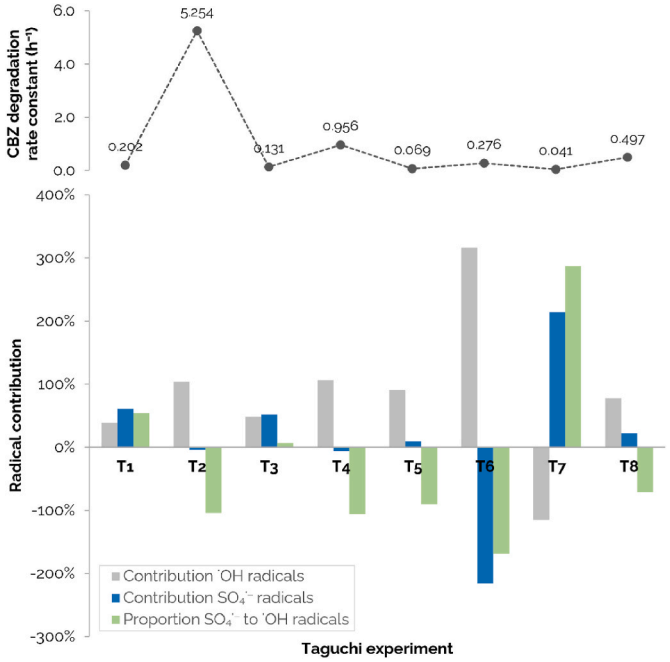

Fig. 3. Estimated contribution of $^{\bullet}OH$ and $SO_4^{\bullet-}$ to the attained CBZ degradation efficiencies per Taguchi experiment. The bars depict the radical contributions and their differential proportion (%), whereas the dots correspond to the observed CBZ degradation rate constant (h^{-1}).

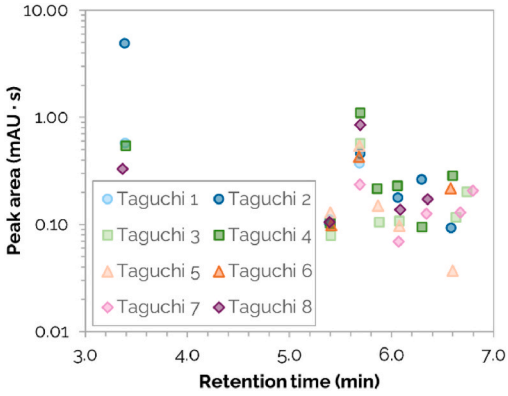

Fig. 4. Comparison of the detected CBZ degradation products after 20 min of treatment per Taguchi experiment, mapped in terms of their retention time (min) and peak area (mAU·s).

slightly higher contributions of $SO_4^{\bullet-}$ (i.e., 61% and −4%, respectively) than in the analogous experiments Taguchi 3 and Taguchi 4 (i.e., 52% and −6%, respectively), where the nucleation side of the polycrystalline BDD was used (i.e., Poly-BDD-N electrode). Accordingly, the proportions of $SO_4^{\bullet-}$ to $^{\bullet}OH$ were higher for the experiments with SC-BDD. Even if this electrode showed negligible sp^2 content (Fig. 2a) in comparison to Poly-BDD-N (Fig. 2c), the observed enhancement of $SO_4^{\bullet-}$ could be attributed to its higher B doping level (Table 2) (Santos et al., 2020). This electrode also showed 1.5- and 5.5-fold higher CBZ degradation rate constants (i.e., 0.202 h^{-1} and 5.254 h^{-1} in experiments Taguchi 1 and Taguchi 2, as opposed to 0.131 h^{-1} and 0.956 h^{-1} in experiments Taguchi 3 and Taguchi 4, respectively).

In terms of the CBZ degradation products formed, the UHPLC chromatograms revealed the presence of a higher number of compounds when the Poly-BDD-N electrode was used. In fact, the Taguchi 3 and 4 scenarios led to the formation of six and seven degradation products, respectively. From these, five compounds seemed to coincide given their similar retention times (namely, the degradation products eluted at around 5.40, 5.69, 5.87, 6.08, and 6.60 min), although their peak intensities were 23–59% lower under the Taguchi 3 conditions. Conversely, the SC-BDD electrode led to three and six CBZ degradation products in the Taguchi 1 and 2 experiments, respectively. From these, three of them presented the same retention time (i.e., 3.39, 5.40, and 5.69 min) but different peak intensities (i.e., 88% lower, 10% higher, and 19% lower in Taguchi 1, respectively). Between these four Taguchi scenarios, only two degradation products were detected in all of them regardless of the operating conditions (i.e., those eluted at 5.40 and 5.69 min). Operating at a higher current density and at a higher SO_4^{2-} concentration led for both electrodes to the highest number of degradation products formed, of which the compounds with retention times 3.39, 5.40, 5.69, 6.08, 6.30 and 6.60 min coincided.

When evaluating the BDD growth side (i.e., Poly-BDD-G electrode) and a commercial BDD (i.e., Poly-BDD-C electrode), the latter led to a higher $SO_4^{\bullet-}$ contribution, being 215% and 22% in experiments Taguchi 7 and Taguchi 8 with respect to 9% and −216% in experiments Taguchi 5 and Taguchi 6, respectively (Fig. 3). Similarly, the $SO_4^{\bullet-}$ proportions with respect to $^{\bullet}OH$ increased for the Poly-BDD-C electrode. Between experiments Taguchi 5 and Taguchi 7, a slight decrease in the CBZ degradation rate constant occurred (i.e., 0.069 h^{-1} and 0.041 h^{-1}, respectively), which is not significant given their low absolute values. Regarding experiments Taguchi 6 and Taguchi 8, a noticeable increase in the $SO_4^{\bullet-}$ contribution was also found together with an increase in the CBZ degradation rate constant (i.e., 0.276 h^{-1} and 0.497 h^{-1}, respectively). Given the similarity between the B doping levels of both electrodes, their difference in behaviour may be largely attributable to the higher sp^2 content of the commercial Poly-BDD-C electrode (Table 2), which has been reported to increase the formation of $SO_4^{\bullet-}$ (de Paiva et al., 2015; dos Santos et al., 2022).

Regarding the degradation products formed, the Poly-BDD-G electrode led to five and three compounds in experiments Taguchi 5 and 6, respectively, whereas the Poly-BDD-C electrode yielded five products for both Taguchi 7 and 8. In the case of the Poly-BDD-G, the three compounds detected in Taguchi 6, i.e., those with retention times 5.40, 5.69, and 6.60 min, were also found in Taguchi 5 although at a peak intensity 30% higher, 27% higher and 83% lower, respectively. For the Poly-BDD-C electrode, only the products eluted at 5.69, 6.08, and 6.34 min were detected regardless of the current density applied and the initial SO_4^{2-} concentration.

3.3. Optimising CBZ degradation

As shown in Fig. 3, the CBZ degradation rate constant was notably higher in experiment Taguchi 2, where $^{\bullet}OH$ were estimated to be dominant (i.e., 104% contribution) and $SO_4^{\bullet-}$ seemed to have a slight detrimental effect (i.e., −4% contribution). This illustrates that CBZ may be more easily degraded by $^{\bullet}OH$ and that $SO_4^{\bullet-}$ may have triggered $^{\bullet}OH$ scavenging reactions (Eqs. (8)–(11)), respectively (Guan et al., 2011; Hadi et al., 2021). When applying the Taguchi method to maximise CBZ degradation kinetics (Fig. 5), its optimal values also corresponded to the Taguchi 2 conditions, that is, degrading CBZ in 500 mg L^{-1} sulfate-containing wastewater, at 50 mA cm^{-2} current density, and via a single-crystal BDD (Fig. 6). For this optimisation target, the current density applied was found to be the most influential factor due to its higher S/N range (i.e., 19.9) and hence with the greatest effect if changed, followed by electrode selection (i.e., S/N range of 17.5). The initial SO_4^{2-} concentration exhibited a considerably lower impact when altering its value (i.e., S/N range of 2.9). Consequently, its selection played a less relevant role in CBZ degradation. In terms of the contributions estimated through ANOVA for the most influential parameters

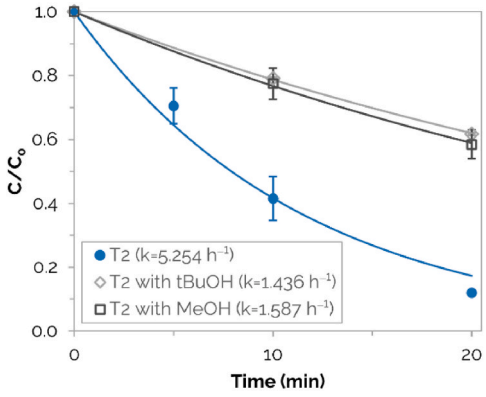

Fig. 6. CBZ degradation during the optimum experiment (with and without scavengers) to maximise the pseudo-first order rate constant, that is, carrying out the degradation with the SC-BDD electrode, in a 500 mg L^{-1} SO_4^{2-} anolyte, and at 50 mA cm^{-2} current density. The acquired degradation rate constants are included in the legend.

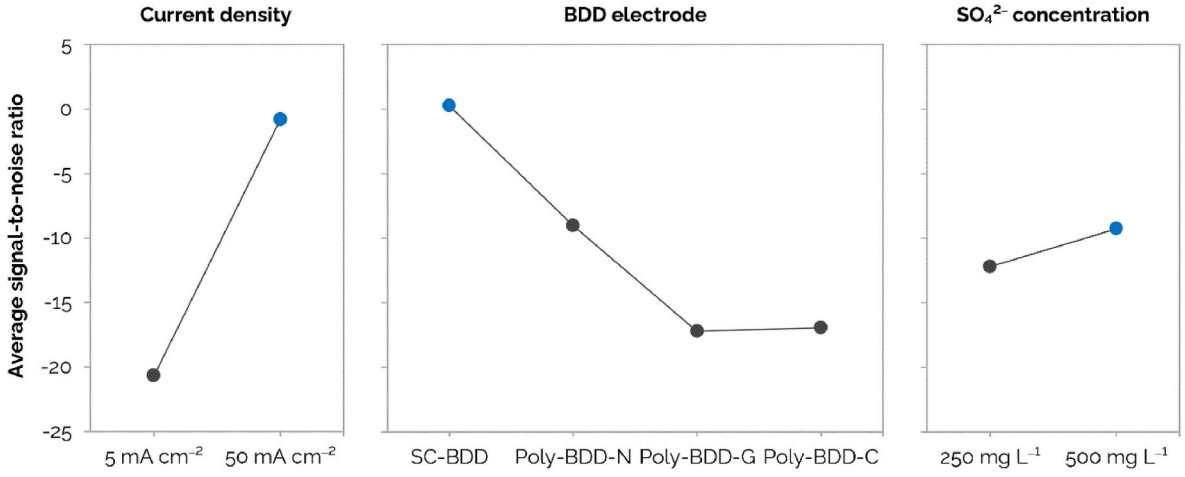

Fig. 5. Taguchi results on average S/N ratios per parameter and level when maximising the CBZ degradation rate constant. Optimum levels are highlighted in blue. Operating parameters are displayed from highest to lowest S/N range and hence on relevance to the optimisation target. (For interpretation of the references to colour in this figure legend, the reader is referred to the Web version of this article.)

(Table B1), the electrode selected and the current density applied contributed to 39.9% and 24.3% of the overall efficiency, respectively.

$$SO_4^{\bullet-} + {}^{\bullet}O\,H \rightarrow HSO_5^- \quad (8)$$

$$SO_4^{\bullet-} + {}^{\bullet}O\,H \rightarrow HSO_4^- + 0.5\,O_2 \quad (9)$$

$$HSO_5^- + {}^{\bullet}O\,H \rightarrow SO_5^{\bullet-} + H_2O \quad (10)$$

$$HSO_5^- + SO_4^{\bullet-} \rightarrow SO_5^{\bullet-} + HSO_4^- \quad (11)$$

The suitability of the elucidated optimal conditions can be argued to be related to the promotion of $^{\bullet}OH$ to degrade CBZ. First, the SC-BDD electrode presented an almost pure sp^3 content, known to favour the formation of $^{\bullet}OH$ (Garcia-Segura et al., 2015; Brito et al., 2018; Espinoza et al., 2019) as well as higher mineralisation efficiencies (Guinea et al., 2009; Medeiros de Araújo et al., 2014; Espinoza et al., 2019) due to its "non-active" behaviour. Second, because the higher values for current density and SO_4^{2-} concentration are also argued to promote the recombination of $SO_4^{\bullet-}$ to form persulfate ions ($S_2O_8^{2-}$), as represented in Eqs. (12) and (13), which may have also led to additional $SO_4^{\bullet-}$ scavenging (Eq. (14)) (Divyapriya and Nidheesh, 2021; Hadi et al., 2021). Finally, a higher current enhances the oxygen evolution reaction, resulting in the formation of hydrogen peroxide (H_2O_2), which can also scavenge $SO_4^{\bullet-}$ (Eqs. (15) and (16)) (Chu et al., 2006). However, in this study, a stainless-steel counter electrode was used, which, as reported in the literature, limits H_2O_2 formation in the absence of a constant supply of air or oxygen into the reaction medium (Medel et al., 2020). Nonetheless, to further validate these observations from previous literature studies, future research should consider the quantification of secondary $S_2O_8^{2-}$ and H_2O_2 species in parallel to the identification and estimation of the different radical contributions. Conversely, the SC-BDD electrode also presented the highest B doping level (Table 2), known to increase the formation of $SO_4^{\bullet-}$. Based on the observed radical contributions, it could be argued that the pure sp^3 content of the SC-BDD electrode was the key parameter determining the distribution of oxidative species formed and/or that its high B doping level promoted $SO_4^{\bullet-}$ formation and recombination mechanisms. As a result, also six degradation products were detected (Fig. A2b) under these conditions.

$$SO_4^{2-} + SO_4^{2-} \rightarrow S_2O_8^{2-} + 2\,e^- \quad (12)$$

$$SO_4^{\bullet-} + SO_4^{\bullet-} \leftarrow\rightarrow S_2O_8^{2-} \quad (13)$$

$$SO_4^{\bullet-} + S_2O_8^{2-} \rightarrow SO_4^{2-} + S_2O_8^{\bullet-} \quad (14)$$

$$SO_4^{\bullet-} + H_2O_2 \rightarrow SO_4^{2-} + H^+ + HO_2^{\bullet} \quad (15)$$

$$SO_4^{\bullet-} + HO_2^{\bullet} \rightarrow SO_4^{2-} + H^+ + O_2 \quad (16)$$

3.4. Optimising the proportion of $SO_4^{\bullet-}$ with respect to $^{\bullet}OH$

For the second optimisation target, i.e., to maximise the proportion of $SO_4^{\bullet-}$ with respect to $^{\bullet}OH$ during CBZ degradation (Eq. (6)), the application of the Taguchi method revealed that optimal operation would correspond to degrading CBZ in 500 mg L^{-1} sulfate-containing wastewater, at 50 mA cm^{-2} current density, and via a commercial polycrystalline BDD (Fig. 7). In this case, the selection of the BDD electrode was the most relevant design consideration (i.e., S/N range of 14.5 and ANOVA contribution of 40.3%), followed by the initial SO_4^{2-} concentration (i.e., S/N range of 9.0 and ANOVA contribution of 2.4%) (Table B2). The current density showed a lower S/N range (i.e., 5.7) but the highest ANOVA contribution (i.e., 43.4%). Additional degradation experiments were conducted under these optimal conditions for the enhanced proportion of $SO_4^{\bullet-}$ (Fig. 8), which led to a CBZ degradation rate constant of 0.467 h^{-1}, an estimated radical contribution of 43% for $^{\bullet}OH$ and 57% for $SO_4^{\bullet-}$ (hence, a differential proportion of 31% for $SO_4^{\bullet-}$), and the formation of six degradation products eluting at 3.39,

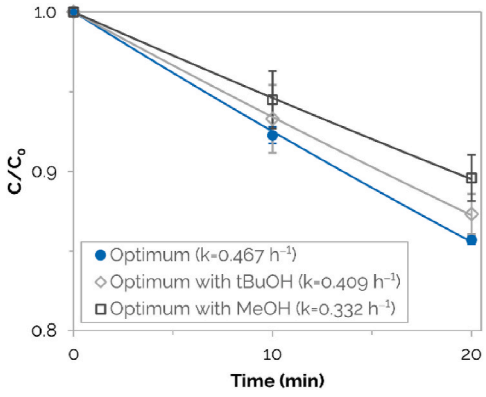

Fig. 8. CBZ degradation during the optimum experiment (with and without scavengers) to maximise the differential proportion of $SO_4^{\bullet-}$, that is, carrying out degradation with the Poly-BDD-C electrode in a 500 mg L^{-1} SO_4^{2-} anolyte and at a 50 mA cm^{-2} current density. The acquired degradation rate constants are included in the legend.

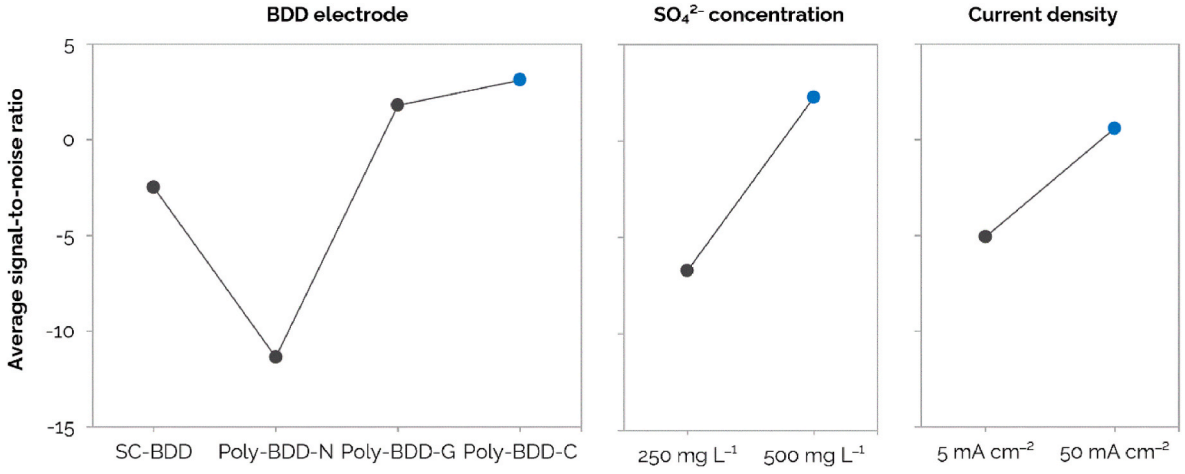

Fig. 7. Taguchi results on average S/N ratios per parameter and level when maximising the differential proportion of $SO_4^{\bullet-}$ during CBZ degradation. Optimum levels are highlighted in blue. Operating parameters are displayed from highest to lowest S/N range and hence on relevance to the optimisation target. (For interpretation of the references to colour in this figure legend, the reader is referred to the Web version of this article.)

5.40, 5.69, 6.08, 6.34, and 6.72 min (Fig. A3).

The suitability of the Poly-BDD-C electrode may be assigned to its relatively high non-diamond content (Fig. 2d) and hence to its "active" nature facilitating adsorption and desorption mechanisms (i.e., enhancing potential SO_4^{2-} adsorption sites favouring $SO_4^{\bullet-}$) as well as showing a lower electrochemical activity due to the oxidation of graphitic carbon impurities (Divyapriya and Nidheesh, 2021; Garcia-Segura et al., 2015). This is aligned with previous observations of higher sp^2 contents favouring $SO_4^{\bullet-}$ formation (de Paiva et al., 2015; dos Santos et al., 2022) as well as increasing $S_2O_8^{2-}$ generation due to the retention of sulfate species on the anode surface (Ganiyu and Martínez-Huitle, 2019). In addition, even if higher B doping levels have been reported to favour the direct electrochemical oxidation of anolyte ions into radicals, operating at high overpotentials also promotes $SO_4^{\bullet-}$ at low B doping levels due to their efficient formation mediated by reaction with $^{\bullet}OH$ (Eq. (2)) (Santos et al., 2020). In fact, this is also related to the elucidation of a higher current density as optimal to boost the proportion of $SO_4^{\bullet-}$ over $^{\bullet}OH$ with the Poly-BDD-C electrode, which presented one of the lowest B doping contents (Table 2). In addition, even if a higher current density and a higher SO_4^{2-} concentration again promoted $S_2O_8^{2-}$ formation (Eqs. (12) and (13)), it can be argued that the reversal reaction in Eq. (13) may have been promoted as well as increased subsequent reactions leading to $^{\bullet}OH$ scavenging and $SO_4^{\bullet-}$ formation (Eqs. (17)–(21)) (Divyapriya and Nidheesh, 2021; Guan et al., 2011; Hadi et al., 2021). The increased current density of the optimum experiment in comparison to the Taguchi 7 experiment was translated into an 11.5-fold increased CBZ degradation rate constant (i.e., from 0.041 h^{-1} to 0.467 h^{-1}). Although in this case the estimated $SO_4^{\bullet-}$ proportion was lower, it should not be taken as an absolute due to the low efficiency of the Taguchi 7 experiment and that the differences with its scavenging scenarios fell within the chromatographic detection limit. Finally, the increased SO_4^{2-} concentration of the optimum experiment in comparison to the Taguchi 8 experiment was primarily reflected in the increased $SO_4^{\bullet-}$ contribution (i.e., from −71% to 31%) at the expense of a 6% reduction in the CBZ degradation rate constant (i.e., from 0.497 h^{-1} to 0.467 h^{-1}).

$$S_2O_8^{2-} + {}^{\bullet}OH \rightarrow S_2O_8^{\bullet-} + OH^- \quad (17)$$

$$S_2O_8^{2-} + {}^{\bullet}OH \rightarrow SO_4^{\bullet-} + HSO_4^- + 0.5\,O_2 \quad (18)$$

$$HSO_4^- + {}^{\bullet}OH \rightarrow SO_4^{\bullet-} + H_2O \quad (19)$$

$$SO_5^{\bullet-} + SO_5^{\bullet-} \rightarrow SO_4^{\bullet-} + SO_4^{\bullet-} + O_2 \quad (20)$$

$$S_2O_8^{2-} + e^- \rightarrow SO_4^{\bullet-} + SO_4^{2-} \quad (21)$$

As depicted in Fig. 7, the Poly-BDD-G electrode was the second best anode material to promote the differential proportion of $SO_4^{\bullet-}$ during CBZ degradation, which is justified by the slightly lower B doping level and lower sp^2 content with respect to Poly-BDD-C (Table 2). On the other hand, SC-BDD would be the next most suitable electrode, possibly due to presenting the highest B doping level, despite its virtually pure sp^3 content. Finally, even if Poly-BDD-N presented a higher sp^2 content and slightly higher B doping level than Poly-BDD-C, it showed the worst performance in promoting $SO_4^{\bullet-}$, which could be related to an increase in radical recombination mechanisms.

4. Discussion of results

This work has, for the first time, explored the implementation of novel single-crystal BDD electrodes for wastewater treatment applications in comparison to polycrystalline morphologies with a diverse set of electrochemical properties (i.e., B doping, sp^3/sp^2 content, microstructure, and roughness). The results showed that the use of a single-crystal BDD (which presented a pure sp^3 diamond content) significantly enhanced the degradation of CBZ, correlated with a predominant $^{\bullet}OH$ contribution. Nonetheless, this electrode also showed the highest B doping level, which could have increased $SO_4^{\bullet-}$ formation and recombination to form $S_2O_8^{2-}$ ions. Alternatively, its high B doping could have been less relevant in the distribution of oxidative species formed in comparison to the presence of pure sp^3 leading to $^{\bullet}OH$. Conversely, a commercial polycrystalline BDD with a relatively high non-diamond (sp^2) content enhanced potential SO_4^{2-} adsorption sites, favouring $SO_4^{\bullet-}$ formation. CBZ degradation was also enhanced when operating at higher SO_4^{2-} concentrations and higher current densities, argued to promote the recombination of $SO_4^{\bullet-}$ and hence increase $^{\bullet}OH$ contributions. On the other hand, a higher SO_4^{2-} concentration and higher current density were also optimal for the differential proportion of $SO_4^{\bullet-}$, given that operating at high overpotentials could enhance $SO_4^{\bullet-}$ formation despite the low B doping level of the commercial polycrystalline BDD used. In this case, it was also argued that even if these conditions promoted $SO_4^{\bullet-}$ recombination, further decomposition of the formed $S_2O_8^{2-}$ could have occurred, promoting $SO_4^{\bullet-}$ formation and $^{\bullet}OH$ scavenging.

In light of further validating the attained observations, it is imperative to further identify and characterise the CBZ degradation products that arise as well as other electrogenerated species (for instance $S_2O_8^{2-}$ and H_2O_2), so that a comprehensive view is achieved regarding the interactions between (novel) BDD material properties, operating conditions, oxidative radical proportions, pollutant degradation mechanisms, and potential effluent toxicity effects.

5. Conclusions

This study has shed light not only on the opportunities for single-crystal BDD electrodes when hydroxyl radicals ($^{\bullet}OH$) are to be promoted but also on how material differences between BDD electrode configurations translate into significant changes in pollutant degradation mechanisms. Therefore, future research in the electrochemical wastewater treatment field should not overlook the characterisation of the anode materials, as their morphological, structural, and electrochemical properties are key factors determining process efficiency and optimisation.

CRediT authorship contribution statement

Sara Feijoo: Writing – review & editing, Writing – original draft, Visualization, Validation, Software, Methodology, Investigation, Formal analysis, Conceptualization. **Simona Baluchová:** Writing – review & editing, Supervision, Resources, Conceptualization. **Mohammadreza Kamali:** Writing – review & editing, Supervision, Conceptualization. **Josephus G. Buijnsters:** Writing – review & editing, Supervision, Resources, Funding acquisition, Conceptualization. **Raf Dewil:** Writing – review & editing, Supervision, Resources, Project administration, Funding acquisition, Conceptualization.

Declaration of competing interest

The authors declare that they have no known competing financial interests or personal relationships that could have appeared to influence the work reported in this paper.

Data availability

Data will be made available on request.

Acknowledgements

This research received funding from the EU Framework Programme for Research and Innovation Horizon 2020 under grant agreement no 861369 (MSCA-ETN InnovEOX) and from the KU Leuven Industrial Research Council under grant number C24E/19/040 (SO4ELECTRIC). S.

B. and J.G.B. acknowledge financial support from the Dutch Research Council (NWO) through the Open Technology Programme (project no 16361). André F. Sartori, Matthias Schreck (University of Augsburg, Germany) and Martin Fischer (Augsburg Diamond Technology GmbH, Germany) are acknowledged for their support with the preparation of the single-crystal BDD electrode, and Clive Hall from Mintres B.V. (Cuijk, The Netherlands) is acknowledged for supplying the free-standing BDD material.

Appendix A. Supplementary data

Supplementary data to this article can be found online at https://doi.org/10.1016/j.envpol.2024.123705.

References

Araújo, K.C.F., dos Santos, E.V., Nidheesh, P.V., Martínez-Huitle, C.A., 2022. Fundamentals and advances on the mechanisms of electrochemical generation of persulfate and sulfate radicals in aqueous medium. Curr. Opin. Chem. Eng. 38, 100870 https://doi.org/10.1016/j.coche.2022.100870.

Beydoun, A., DuPont, S., Zhou, D., Matta, M., Nagire, V., Lagae, L., 2020. Current role of carbamazepine and oxcarbazepine in the management of epilepsy. Seizure 83, 251–263. https://doi.org/10.1016/j.seizure.2020.10.018.

Brito, C.N., Ferreira, M.B., de O. Marcionilio, S.M.L., de Moura Santos, E.C.M., Linares Léon, J.J., Ganiyu, S.O., Martínez-Huitle, C.A., 2018. Electrochemical oxidation of Acid Violet 7 dye by using Si/BDD and Nb/BDD electrodes. J. Electrochem. Soc. 165 (5), E250. doi:10.1149/2.1111805jes.

Čambal, P., Baluchová, S., Taylor, A., Míka, L., Vondráček, M., Gedeonová, Z., Hubík, P., Mortet, V., Schwarzová-Pecková, K., 2023. Boron-doped {113}, {115} and {118}-oriented single- crystal diamond electrodes: effect of surface pre-treatment. Electrochim. Acta 469, 143214. https://doi.org/10.1016/j.electacta.2023.143214.

Cañizares, P., Sáez, C., Martínez, F., Rodrigo, M., 2008. The role of the characteristics of p-Si BDD anodes on the efficiency of wastewater electro-oxidation processes. Electrochem. Solid State Lett. 11 (7), E15. https://doi.org/10.1149/1.2916436.

Chu, W., Lau, T.K., Fung, S.C., 2006. Effects of combined and sequential addition of dual oxidants (H_2O_2/$S_2O_8^{2-}$) on the aqueous carbofuran photodegradation. J. Agric. Food Chem. 54 (26), 10047–10052. https://doi.org/10.1021/jf062018k.

Divyapriya, G., Nidheesh, P., 2021. Electrochemically generated sulfate radicals by boron doped diamond and its environmental applications. Curr. Opin. Solid State Mater. Sci. 25 (3), 100921 https://doi.org/10.1016/j.cossms.2021.100921.

Duan, X., Niu, X., Gao, J., Wac lawek, S., Tang, L., Dionysiou, D.D., 2022. Comparison of sulfate radical with other reactive species. Curr. Opin. Chem. Eng. 38, 100867 https://doi.org/10.1016/j.coche.2022.100867.

Espinoza, L.C., Aranda, M., Contreras, D., Henríquez, A., Salazar, R., 2019. Effect of the sp^3/sp^2 ratio in boron-doped diamond electrodes on the degradation pathway of aniline by anodic oxidation. Chemelectrochem 6 (18), 4801–4810. https://doi.org/10.1002/celc.201901218.

European Commission, 2022. Council Directive of 3 November 1998 on the quality of water intended for human consumption (98/83/EC). OJ L 330, 5.12.1998, p. 32–54. http://data.europa.eu/eli/dir/1998/83/oj.

Feijoo, S., Kamali, M., Pham, Q.-K., Assoumani, A., Lestremau, F., Cabooter, D., Dewil, R., 2022a. Electrochemical Advanced Oxidation of carbamazepine: mechanism and optimal operating conditions. Chem. Eng. J. 446, 137114 https://doi.org/10.1016/j.cej.2022.137114.

Feijoo, S., Kamali, M., Dewil, R., 2022b. Effects of wastewater composition and reactor operating mode on the removal of micropollutants via electrochemical advanced oxidation. J. Water Process Eng. 50, 103220 https://doi.org/10.1016/j.jwpe.2022.103220.

Ganiyu, S.O., Martínez-Huitle, C.A., 2019. Nature, mechanisms and reactivity of electrogenerated reactive species at thin-film boron-doped diamond (BDD) electrodes during electrochemical wastewater treatment. Chemelectrochem 6 (9), 2379–2392. https://doi.org/10.1002/celc.201900159.

Ganiyu, S.O., Martínez-Huitle, C.A., Oturan, M.A., 2021. Electrochemical advanced oxidation processes for wastewater treatment: advances in formation and detection of reactive species and mechanisms. Curr. Opin. Electrochem. 27, 100678 https://doi.org/10.1016/j.coelec.2020.100678.

Garcia-Segura, S., Vieira dos Santos, E., Martínez-Huitle, C.A., 2015. Role of sp^3/sp^2 ratio on the electrocatalytic properties of boron-doped diamond electrodes: a mini review. Electrochem. Comm. 59, 52–55. https://doi.org/10.1016/j.elecom.2015.07.002.

Guan, Y.-H., Ma, J., Li, X.-C., Fang, J.-Y., Chen, L.-W., 2011. Influence of pH on the formation of sulfate and hydroxyl radicals in the UV/Peroxymonosulfate system. Environ. Sci. Technol. 45 (21), 9308–9314. https://doi.org/10.1021/es2017363.

Guinea, E., Centellas, F., Brillas, E., Cañizares, P., Sáez, C., Rodrigo, M.A., 2009. Electrocatalytic properties of diamond in the oxidation of a persistant pollutant. Appl. Catal. B Environ. 89 (3), 645–650. https://doi.org/10.1016/j.apcatb.2009.01.028.

Hadi, S., Taheri, E., Amin, M.M., Fatehizadeh, A., Aminabhavi, T.M., 2021. Advanced oxidation of 4-chlorophenol via combined pulsed light and sulfate radicals methods: effect of co-existing anions. J. Environ. Manage 291, 112595. https://doi.org/10.1016/j.jenvman.2021.112595.

Ivandini, T.A., Watanabe, T., Matsui, T., Ootani, Y., Iizuka, S., Toyoshima, R., Kodama, H., Kondoh, H., Tateyama, Y., Einaga, Y., 2019. Influence of surface orientation on electrochemical properties of boron-doped diamond. J. Phys. Chem. C 123 (9), 5336–5344. https://doi.org/10.1021/acs.jpcc.8b10406.

Jiang, W., Xia, T., Yun, Y., Li, M., Zhang, F., Gao, S., Chen, W., 2019. UHPLC-MS/MS method for simultaneous determination of carbamazepine and its seven major metabolites in serum of epileptic patients. J. Chromatogr. B 1108, 17–24. https://doi.org/10.1016/j.jchromb.2018.12.016.

Li, X., Fan, S., Jin, C., Gao, M., Zhao, Y., Guo, L., Ji, J., She, Z., 2022a. Electrochemical degradation of tetracycline hydrochloride in sulfate solutions on boron-doped diamond electrode: the accumulation and transformation of persulfate. Chemosphere 305, 135448. https://doi.org/10.1016/j.chemosphere.2022.135448.

Li, Y., Yang, Z., Yang, K., Wei, J., Li, Z., Ma, C., Yang, X., Wang, T., Zeng, G., Yu, G., Yu, Z., Zhang, C., 2022b. Removal of chloride from water and wastewater: removal mechanisms and recent trends. Sci. Total Environ. 821, 153174 https://doi.org/10.1016/j.scitotenv.2022.153174.

Liu, Z., Baluchová, S., Sartori, A.F., Li, Z., Gonzalez-Garcia, Y., Schreck, M., Buijnsters, J. G., 2023. Heavily boron-doped diamond grown on scalable heteroepitaxial quasi-substrates: a promising single crystal material for electrochemical sensing applications. Carbon 201, 1229–1240. https://doi.org/10.1016/j.carbon.2022.10.023.

Liu, Z., Baluchová, S., Li, Z., Gonzalez-Garcia, Y., Hall, C.E., Buijnsters, J.G., 2024. Unravelling microstructure-electroactivity relationships in free-standing polycrystalline boron-doped diamond: a mapping study. Acta Mater. 266, 119671 https://doi.org/10.1016/j.actamat.2024.119671.

Mandal, N., Doloi, B., Mondal, B., Das, R., 2011. Optimization of flank wear using Zirconia Toughened Alumina (ZTA) cutting tool: Taguchi method and regression analysis. Measurement 44 (10), 2149–2155. https://doi.org/10.1016/j.measurement.2011.07.022.

Medeiros de Araújo, D., Cañizares, P., Martínez-Huitle, C.A., Rodrigo, M.A., 2014. Electrochemical conversion/combustion of a model organic pollutant on BDD anode: role of sp^3/sp^2 ratio. Electrochem. Commun. 47, 37–40. https://doi.org/10.1016/j.elecom.2014.07.017.

Medel, A., Treviño-Reséndez, J., Brillas, E., Meas, Y., Sirés, I., 2020. Contribution of cathodic hydroxyl radical generation to the enhancement of electro-oxidation process for water decontamination. Electrochim. Acta 331. https://doi.org/10.1016/j.electacta.2019.135382.

Mortet, V., Gregora, I., Taylor, A., Lambert, N., Ashcheulov, P., Gedeonova, Z., Hubik, P., 2020. New perspectives for heavily boron-doped diamond Raman spectrum analysis. Carbon 168, 319–327. https://doi.org/10.1016/j.carbon.2020.06.075.

NORMAN-Network, 2021. NORMAN database system. https://www.norman-network.com/nds.

Ogulata, R.T., Mezarcioz, S.M., 2011. Optimization of air permeability of knit- ted fabrics with the Taguchi approach. J. Text. Inst. 102 (5), 395–404. https://doi.org/10.1080/00405000.2010.482347.

de Paiva Barreto, J.P., de Freitas Araújo, K.C., de Araújo, D.M., Martínez-Huitle, C.A., 2015. Effect of sp^3/sp^2 ratio on boron doped diamond films for producing persulfate. ECS Electrochem. Lett. 4 (12), E9. https://doi.org/10.1149/2.0061512eel.

Preethi, S.P., Shanmugavel, G., Kumar, Y.K., N, G., M, R.B.J., 2023. Recent progress in mineralization of emerging contaminants by advanced oxidation process: a review. Environ. Pollut., 122842 https://doi.org/10.1016/j.envpol.2023.122842.

R Core Team, R., 2023. A Language and Environment for Statistical Computing. R Foundation for Statistical Computing, Vienna, Austria. https://www.R-project.org/.

Radjenovic, J., Petrovic, M., 2017. Removal of sulfamethoxazole by electrochemically activated sulfate: implications of chloride addition. J. Hazard Mater. 333, 242–249. https://doi.org/10.1016/j.jhazmat.2017.03.040.

Rizzo, L., Malato, S., Antakyali, D., Beretsou, V.G., Đolić, M.B., Gernjak, W., Heath, E., Ivancev-Tumbas, I., Karaolia, P., Lado Ribeiro, A.R., Mascolo, G., McArdell, C.S., Schaar, H., Silva, A.M.T., Fatta-Kassinos, D., 2019. Consolidated vs new advanced treatment methods for the removal of contaminants of emerging concern from urban wastewater. Sci. Total Environ. 655, 986–1008. https://doi.org/10.1016/j.scitotenv.2018.11.265.

Santos, G.O., Eguiluz, K.I., Salazar-Banda, G.R., Sáez, C., Rodrigo, M.A., 2020. Understanding the electrolytic generation of sulfate and chlorine oxidative species with different boron-doped diamond anodes. J. Electroanal. Chem. 857, 113756 https://doi.org/10.1016/j.jelechem.2019.113756.

dos Santos, A.J., Fortunato, G.V., Kronka, M.S., Vernasqui, L.G., Ferreira, N.G., Lanza, M. R., 2022. Electrochemical oxidation of ciprofloxacin in different aqueous matrices using synthesized boron-doped micro and nano-diamond anodes. Environ. Res. 204, 112027 https://doi.org/10.1016/j.envres.2021.112027.

Scaria, J., Nidheesh, P.V., 2022. Comparison of hydroxyl-radical-based advanced oxidation processes with sulfate radical-based advanced oxidation processes. Curr. Opin. Chem. Eng. 36, 100830 https://doi.org/10.1016/j.coche.2022.100830.

Sidorov, V., Ekimov, E., 2010. Superconductivity in diamond. Diam. Relat. Mater. 19 (5), 351–357. https://doi.org/10.1016/j.diamond.2009.12.002.

da Silva, S.W., Navarro, E.M., Rodrigues, M.A., Bernardes, A.M., Pérez-Herranz, V., 2018. The role of the anode material and water matrix in the electrochemical oxidation of norfloxacin. Chemosphere 210, 615–623. https://doi.org/10.1016/j.chemosphere.2018.07.057.

Suresh Babu, D., Mol, J.M., Buijnsters, J.G., 2022. Experimental insights into anodic oxidation of hexafluoropropylene oxide dimer acid (GenX) on boron-doped diamond anodes. Chemosphere 288, 132417. https://doi.org/10.1016/j.chemosphere.2021.132417.

Wang, J., Wang, S., 2020. Reactive species in advanced oxidation processes: formation, identification and reaction mechanism. Chem. Eng. J. 401, 126158 https://doi.org/10.1016/j.cej.2020.126158.

Wilkinson, J.L., Boxall, A.B.A., Kolpin, D.W., et al., 2022. Pharmaceutical pollution of the world's rivers. Proc. Natl. Acad. Sci. USA 119 (8). https://doi.org/10.1073/pnas.2113947119.

Yakamercan, E., Bhatt, P., Aygun, A., Adesope, A.W., Simsek, H., 2023. Comprehensive understanding of electrochemical treatment systems combined with biological processes for wastewater remediation. Environ. Pollut. 330, 121680 https://doi.org/10.1016/j.envpol.2023.121680.